

Scaling Limits of Memristor-Based Routers for Asynchronous Neuromorphic Systems

Junren Chen, Siyao Yang, Huaqiang Wu, *Senior Member, IEEE*, Giacomo Indiveri, *Senior Member, IEEE*, Melika Payvand, *Member, IEEE*

Abstract—Multi-core neuromorphic systems typically use on-chip routers to transmit spikes among cores. These routers require significant memory resources and consume a large part of the overall system’s energy budget. A promising alternative approach to using standard CMOS and SRAM-based routers is to exploit the features of memristive crossbar arrays and use them as programmable switch-matrices that route spikes. However, the scaling of these crossbar arrays presents physical challenges, such as “IR drop” on the metal lines due to the parasitic resistance, and leakage current accumulation on multiple active memristors in their “off” state. While reliability challenges of this type have been extensively studied in synchronous systems for compute-in-memory matrix-vector multiplication (MVM) accelerators and storage class memory, little effort has been devoted so far to characterizing the scaling limits of memristor-based crossbar routers. Here, we study the challenges of memristive crossbar arrays, when used as routing channels to transmit spikes in asynchronous Spiking Neural Network (SNN) hardware. We validate our analytical findings with experimental results obtained from a 4K-ReRAM chip which demonstrates its functionality as a routing crossbar. We determine the functionality bounds on the routing due to the IR drop and leak problem, based on theoretical modeling, circuit simulations for a 22 nm FDSOI technology, and experimental measurements. This work highlights the limitations of this approach and provides useful guidelines for engineering the memristor device properties in memristive crossbar routers for multi-core asynchronous neuromorphic systems.

Index Terms—Memristor crossbar, router, reliability, scaling, IR drop, leakage, on/off ratio, asynchronous, neuromorphic

I. INTRODUCTION

WHILE memristive devices have been often used in neuromorphic systems to emulate synaptic functions [1], [2], their non-volatile memory features can also be exploited to configure and re-program the connectivity between digital logic elements [3]–[5]. This memristor-based routing approach can also be used in multi-core Spiking Neural Network (SNN) neuromorphic processors, in which neurons communicate with each other via all-or-none spike events [6], [7]. Memristive crossbar routers act as distributed switch matrices which allow the digital spikes to be transmitted or get blocked, thus resulting in programming and storing the connectivity of the SNN between multiple processing cores (Fig. 1). This approach can be particularly advantageous for reducing static power

This work won the Best Paper Award at the 2023 30th IEEE International Conference on Electronics, Circuits and Systems (ICECS).

Junren Chen, Giacomo Indiveri and Melika Payvand are with the Institute of Neuroinformatics, University of Zurich and ETH Zurich, 8057 Zurich, Switzerland (e-mail: junren@ini.uzh.ch).

Siyao Yang and Huaqiang Wu are with the School of Integrated Circuits, Tsinghua University, 100084 Beijing, China.

Manuscript received MONTH DD, 2023; revised MONTH DD, YEAR.

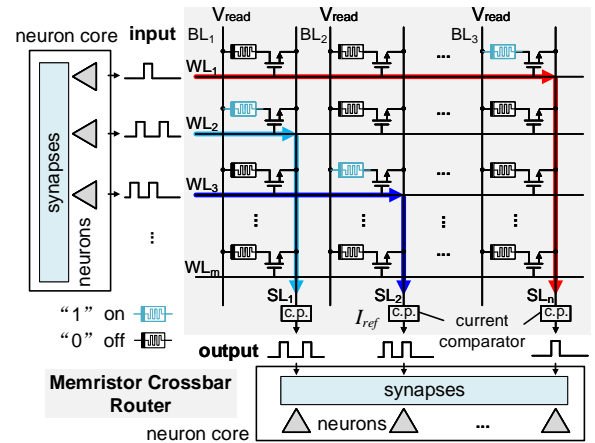


Fig. 1. Schematic diagram of a memristor-based switch-matrix for transmitting voltage pulses (spikes) across neural cores, using 1-transistor-1-memristor (1T1R) crossbars. One column represents a single routing channel. V_{read} is applied to read the cells at the arrival of input pulses on WLS. If the current on SL is greater than a reference (I_{ref}), the current comparator (c.p.) generates an output pulse, otherwise, the output remains at zero voltage. Thus, the “on” state, i.e., Low Resistance State (LRS), of the memristor enables the propagation of the input spikes, while the “off” state, i.e., High Resistance State (HRS), blocks them.

consumption, thanks to the very low static power consumption of resistive memory, and to their non-volatility. As static power consumption accounts for a large proportion of the power budget in CMOS memories implemented in advanced technologies nodes [8], memristive routers represent a promising alternative for building multi-core SNN processors on stringent power budgets (e.g. for edge-computing applications).

To scale the fan-in/out of the neurons while keeping the memory resources at minimum, it is however important to leverage the temporal sparsity of SNNs so that routing channels can be used as shared resources for multiple neurons. A theoretical reliability study of the trade-off between fan-in/out of an SNN node and transmission collision probability in a routing channel as a function of array size has already been reported in [9]. This study has also characterized the reliability of signal transmission with respect to the on/off ratio (R_{on}/R_{off}) of individual memristive devices. In this work, we extend this study with both further analysis on the scaling of memristive routing arrays, and by performing experimental measurements on a fabricated 4K-ReRAM chip. Specifically we first experimentally demonstrate the ability of a memristor crossbar router to transmit spikes, and characterize its scaling reliability with respect to the leakage current accumulation

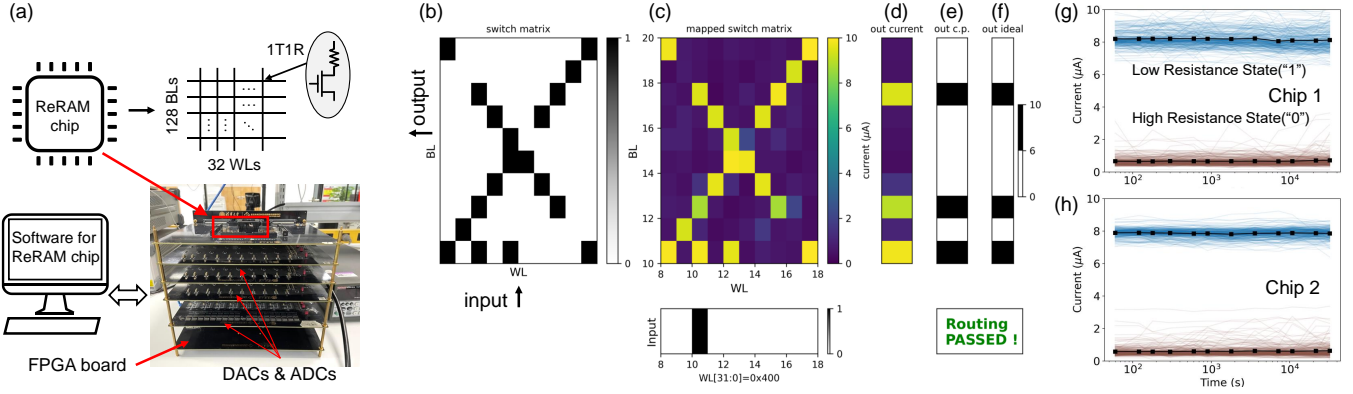


Fig. 2. Experimental demonstration of routing spikes on a memristor crossbar chip. (a) The measurement system of a 4K-cell ReRAM chip. (b) An arbitrary switch matrix pattern. The black squares indicate the cross points that connect the corresponding inputs and outputs. (c) The mapped switch matrix on the hardware crossbar array. The colors show the currents from each cell (read at $0.2V$). (d) Read out currents at the arrival of an input spike. Input spike on WL_{10} is multicast to three receivers (e.g. neurons). (e) The output currents quantified by a threshold ($6\mu A$), which simulates the function of a current comparator (c.p.). (f) The ideal correct output pulses corresponding to applying the input on the switch matrix in (b). If (e) matches (f), the routing is successful (“passed”), otherwise the routing is “failed” due to transmission errors. (g)&(h) Retention measurements of binary ReRAM cells of two different chips at room temperature, demonstrating the reliability of the memory devices for binary operation and chip-to-chip variability. Black lines show the mean values (for 256 cells/state).

from “off” cells. Next, we present a quantitative analysis, using both theoretical considerations and circuit simulations, on the issue of scaling due to “IR drop” as a result of the line parasitics. Finally, we evaluate the influence of leakage current from MOSFETs when scaling down to 22 nm technology. We conclude by providing guidelines and specifications on the memristor properties required for enabling the scaling of neuromorphic processing systems that use memristor-based routing schemes.

It is worth noting that while the memristor crossbar router in this work is specific to SNN hardware, the routing approach and principles discussed may find broader applications.

II. EXPERIMENTAL MEASUREMENTS

A. Memristor Crossbar Router on a ReRAM Chip

The experimental measurements were made using non-volatile 1T1R HfO_x -based Resistive Random Access Memory (ReRAM) chips integrating 32×128 (4K) cells. An FPGA board in the measurement system supports over two hundred pins of the ReRAM chip operating in parallel, which provides very high flexibility and test capacity. For instance, 32 WLS can be operated individually and in parallel. The system supports parallel read out. It can flexibly implement unicast, multicast and broadcast communication by programming one, multiple or all cells on the same input Word Line (WL) to “on” state, respectively. This feature is key for enabling the use of a chip as crossbar router demonstrator. Figure 2 shows the experimental set up and demonstrates routing spikes through the ReRAM chip. Note that the presentation of the crossbar (WL, BL locations) in Fig. 2 is rotated 90° compared to Fig. 1. The input/output directions are labeled accordingly for the clarification. An arbitrary switch matrix (b) is mapped on the array (c), and an input spike on WL_{10} is sent to three receivers. Since the c.p. output (e) matches the ideal output (f), routing is successful. The retention of binary cells of two different chips (g, h) show the reliability of ReRAM cells.

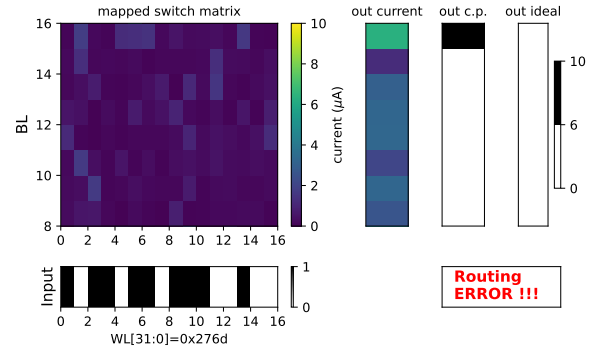


Fig. 3. A measurement showing that when nine simultaneous input pulses arrive and all cells are in “off” state, an undesired error output pulse is generated.

B. Undesired Output Pulses from “Off” Cells

The leakage from the active WLS of the crossbar array with “off” cells can pose a reliability issue. When multiple input pulses arrive at the same time, an undesired error pulse will be generated, if the accumulated current on a SL from “off” cells is higher than the threshold of c.p. (I_{ref}). This issue indicates a minimum on/off ratio requirement of memristors to avoid transmission errors, as determined also in our previous work [9]. Here, we experimentally measure the occurrence of these errors (see Fig. 3) for a case in which nine simultaneous input pulses arrive and all cells are programmed to “off” state. In this experiment, on the bit-line BL_{15} , the accumulated “off” leakage currents is higher than the threshold ($6\mu A$), so an output routing pulse is generated, even though no valid routing path exists.

III. SCALING ANALYSIS

In addition to the leak accumulation problem, the IR drop on the metal lines poses a challenge for scaling memristor

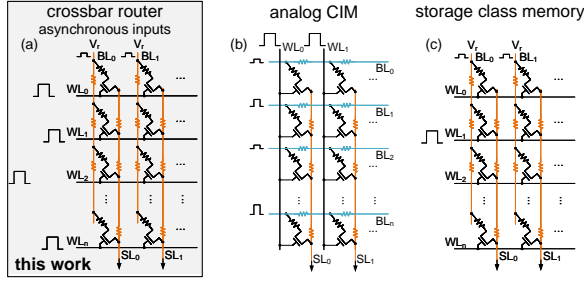


Fig. 4. IR drop pathways for different applications. (a) Crossbar router diagram: transmitting asynchronous voltage pulses. (b) Compute-in-memory (CIM) MVM accelerators in synchronous system: fully parallel computing. (c) Storage class memory: only one WL is activated in a read operation in synchronous/asynchronous system.

crossbars. In the crossbar router case, it decreases the read margin between “on” and “off” states.

A. IR Drop Analysis

Figure 4 shows the IR drop paths on 1T1R array with different WL, Bit Line (BL) and Source Line (SL) arrangements. The input patterns differentiate between different applications. IR drop reliability issues on CIM MVM accelerators and storage class memory have been extensively studied in previous works, e.g. [10]–[12]. For our crossbar router use case (Fig. 4 (a)), we evaluate the routing error probability caused by current accumulation from “off” cells as a function of the network/router scaling.

Due to the IR drop, the read voltage applied to the memory cells down the line will be lower than the one applied, resulting in lower output currents, and hence resulting in a possible output error in the corresponding routing channel. This is illustrated in Fig. 5. For example, when reading a cell which stores a “1”, and expecting to transmit the input pulse to the corresponding output. There will be an error if the IR drop leads to $I_{SL} < I_{ref}$, as no output voltage pulse will be generated. Since the IR drop only has the effect of decreasing the values of I_{SL} , it will not cause errors for “0” cases, so we restrict our analysis to the reading of “1” cases.

In the example shown in Fig. 5 (a), only one spike arrives to the channel on one R_{on} (WL_i). Assuming $n > j > i$,

$$I_{SL}^1 = \frac{V_{read}}{ir + R_{on} + (n-i)r} = \frac{V_{read}}{R_{on} + nr} \quad (1)$$

where r is the line resistance between two adjacent cells. R_{on} is the resistance of a “on” cell.

In the example of Fig. 5 (b), when two spikes arrive: WL_i is switched on, while another R_{off} (WL_j) is on,

$$I_{SL}^2 = \frac{V_{read}}{ir + [R_{on} + (j-i)r]/[(j-i)r + R_{off}] + (n-j)r} \quad (2)$$

Since $[R_{on} + (j-i)r]/[(j-i)r + R_{off}] < R_{on} + (j-i)r$, we can derive:

$$I_{SL}^2 > \frac{V_{read}}{ir + R_{on} + (j-i)r + (n-j)r} = \frac{V_{read}}{R_{on} + nr} = I_{SL}^1 \quad (3)$$

We get $I_{SL}^2 > I_{SL}^1$. Accordingly, $I_{SL}^n > \dots > I_{SL}^3 > I_{SL}^2 > I_{SL}^1$, n means n cells are simultaneously activated. If R_{off}

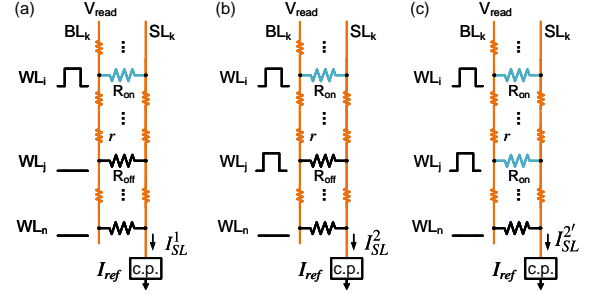


Fig. 5. IR drop model of one routing channel. r is the unit line resistance. (a) Only one R_{on} is switched on. (b) One R_{on} and one R_{off} are switched on at the same time. (c) Two R_{on} are switched on at the same time.

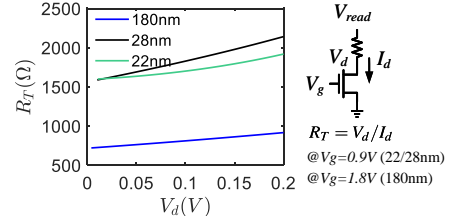


Fig. 6. Resistance of transistor in 1T1R cells in different technology nodes. Simulation based on PDK from foundries. Transistor size is chosen with proper driving capacity for programming memristors ($> 150\mu A$).

in eq. 2 is replaced with R_{on} , i.e. case Fig. 5 (c), we can get the same result that $I_{SL}^n > \dots > I_{SL}^3 > I_{SL}^2 > I_{SL}^1$. It means that any additional cells (either R_{off} or R_{on}) in the same channel are switched on with one “on” path, the resultant output current on the SL is higher than I_{SL}^1 . So, as long as I_{SL}^1 is able to produce a correct routing output, i.e. the condition $I_{SL}^1 > I_{ref}$ holds, any additional simultaneous inputs will not lead to errors, no matter how big r is.

Thus, for what concerns the input patterns, simultaneous inputs do not cause routing errors due to IR drop. The impact of IR drop on the functionality of the crossbar router that we need to assess is the margin to separate a “on” cell and the accumulation of multiple “off” ones.

Defining the on/off (or in our case off/on) ratio of fabricated memristors as $k = R_{off}/R_{on} > 1$. The physical sensing circuit at the end of SL or BL has to always take into account also the resistance of the metal line (nr). So, the real on/off ratio of memristors relevant for the sensing circuit becomes $k' = (R_{off} + nr)/(R_{on} + nr)$. It should be noted that practically, k' is the ratio of the reference current of sensing circuit to the current of “off” cells, not exactly “on” cell to “off” cell when device-to-device variation is factored in.

The relationship between k and k' is

$$k' = \frac{kR_{on} + nr}{R_{on} + nr} = \frac{(k-1)R_{on} + R_{on} + nr}{R_{on} + nr} = \frac{k-1}{1 + nr/R_{on}} + 1 \quad (4)$$

Since $1 + nr/R_{on} > 1$, $\frac{k-1}{1 + nr/R_{on}} < k-1$, $k' < k$. As the router size scales up and the metal pitch of the fabrication technology scales down, IR drop increases and on/off ratio decreases. For example, if $nr = R_{on}$, the on/off ratio to sensing circuit is $k' = k/2 + 1/2$. The sensing window (SW) is halved. IR drop lowers SW, which can increase error probability caused by accumulated currents from “off” cells.

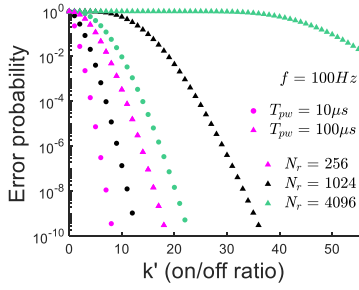


Fig. 7. Probability of an undesired error output pulse due to accumulated “off” currents, with independent Poisson input pulse trains. k' implies the number of simultaneous inputs that can be tolerated, f is the frequency of each input, T_{pw} is the routing pulse width, N_r is the size of the crossbar.

B. Influence of Resistance in Transistors

In practice, to engineer the proper resistance range of memristors and their scaling ability (limited by IR drop and on/off ratio requirement) for routing application in the 1T1R scheme of Fig. 1, the resistance of transistors in routing mode (when reading memristors) should be taken into account. We can therefore reformulate eq. 4 as

$$k' = \frac{R_{off} + R_T + nr}{R_{on} + R_T + nr} = \frac{k - 1}{1 + (R_T + nr)/R_{on}} + 1 \quad (5)$$

R_T is the resistance from a transistor. Figure 6 shows R_T values in different technology nodes. In 22 nm and 28 nm technology nodes $R_T \approx 1.7 k\Omega$. $r \approx 2.5 \Omega$, as estimated from the 4K ReRAM chip layout.

C. Scaling of Error Probability

As the size of the router increases, the minimum on/off ratio required increases, due to higher probability of simultaneous inputs, as shown in Fig. 7. The theory of modeling the relationship between error probability, input frequencies, routing pulse width and the requirement of on/off ratio was presented in [9]. The longer the pulse width, the higher the probability that more simultaneous pulses occur in T_{pw} , causing more memristor leakage current accumulation. For pulse widths (T_{pw}) between 100 ns to a few μs (e.g. neuromorphic circuits in sub-threshold [13]), and for large crossbar arrays ($N_r = 4096$), the requirement of k' is about 20, to achieve error probability $< 10^{-10}$. For shorter T_{pw} values of a few ns to tens of ns (e.g. above-threshold analog circuits in mixed-signal systems, or digital circuits), $k' = 10$ can be used, reducing the error probability to $\ll 10^{-10}$.

Figure 8 shows the scaling of sensing margin (k'/k) with router size and r , where R_{on} is more dominant than k . Increasing sensing margin at the cost of lowering R_{on} is not an effective solution, because low R_{on} ($< 10 k\Omega$) suffers serious IR drop. Instead, R_{off} should increase. In 22/28 nm technology, line resistance effect is negligible for $N_r < 512$ when $R_{on} > 10 k\Omega$.

To support 1K inputs ($R_T \approx 1.7 k\Omega$, $nr \approx 2.5 k\Omega$), and to achieve relatively high k' around 10, $R_{on} > 10 k\Omega$, $R_{off} > 200 k\Omega$ is required. In engineering devices with on/off ratio of approximately 20, a resistance range of hundreds $k\Omega$ to $M\Omega$

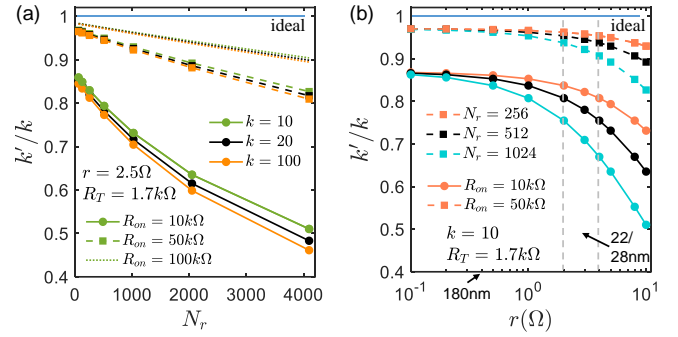


Fig. 8. The scaling of sensing margin with (a) router size N_r and (b) line resistance r . R_{on} is more dominant than k . When $N_r < 512$, in 22/28 nm technology nodes ($r \approx 2.5 \Omega$), the line resistance is negligible.

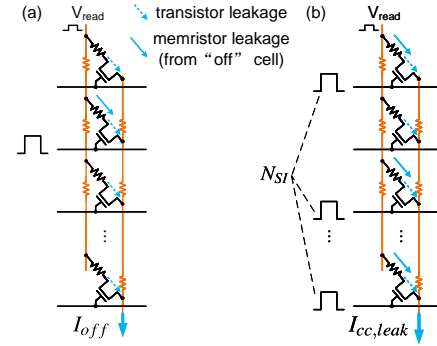


Fig. 9. Illustration of leakage current accumulation from transistors and “off” memristors when input pulses arrive. (a) I_{off} is the resulting current from one input at R_{off} . (b) $I_{cc,leak}$ is the overall “off” currents on a channel corresponding to the arrival of N_{SI} simultaneous inputs.

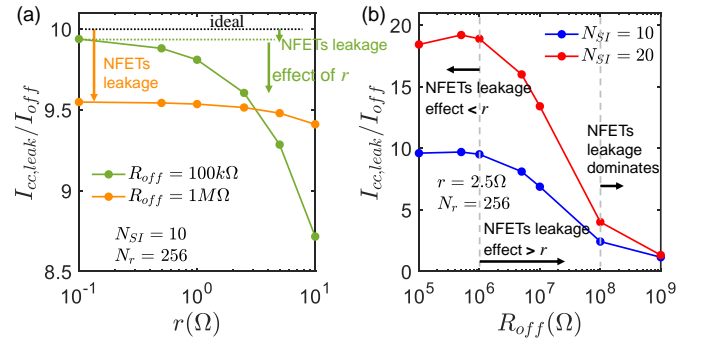


Fig. 10. The effect of line resistance and leakage currents from NFETs (22 nm FDSOI) in 1T1R array when “off” cells receive simultaneous input pulses. (a) IR drop effect on the overall “off” currents $I_{cc,leak}$ of N_{SI} simultaneous inputs. The lower the $I_{cc,leak}$, the lower the leakage power consumption and higher the routing reliability. (b) The influence of NFETs leakage vs. line resistance effect as R_{off} increases.

is preferable (e.g. $R_{on} = 50 k\Omega$, $R_{off} = 1 M\Omega$). For mixed-signal neuromorphic chips that use circuits operating in the sub-threshold or weak-inversion regime, resistance ranges of $M\Omega$ for routing spikes are preferable. This takes advantage of the fact that these neuromorphic circuits typically have slow time constants, so the corresponding routers have less stringent speed margins and lower power requirements.

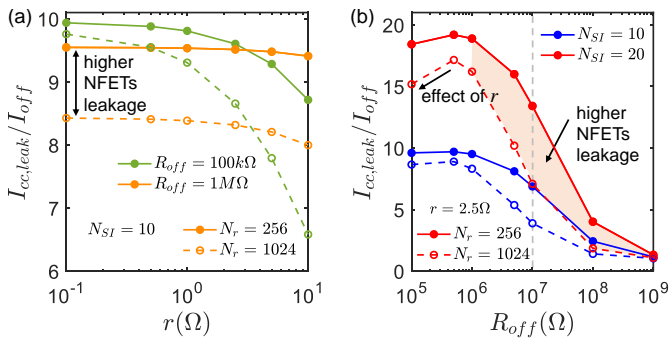


Fig. 11. Joint effects of IR drop and transistor leakage when the router size scales up from 256 to 1024.

D. Effect of Transistor Leakage Currents

When including transistors and line resistance in SPICE simulation (using a normal threshold NFET of 22 nm FDSOI technology), transistor leakage and IR drop play concurrent roles in overall leakage current accumulation when the router receives inputs. The corresponding schematic is shown in Fig. 9. The difference between $I_{cc,leak}/I_{off}$ and N_{SI} indicates the influence by NFETs leakage and IR drop. The overall leakage current from 256 NFETs in one channel is about $10 nA$. Leakage currents from NFETs have little effects when $R_{off} < 1 M\Omega$ in Fig. 10 (a), but they overpower currents from “off” cells when $R_{off} > 100 M\Omega$ in Fig. 10 (b). Figure 10 (a) also shows that the accumulated currents from N_{SI} “off” cells ($I_{cc,leak}$) in a channel is lower than $N_{SI} \times I_{off}$ (ideal) due to IR drop, which slightly enlarge the sensing window of distinguishing from R_{on} compared to the ideal case. In other words, IR drop lowers $I_{cc,leak}$ and alleviates reliability issue regarding accumulation of I_{off} . But this alleviation is trivial when $R_{off} > 1 M\Omega$.

As the router size scales up from 256 to 1024, as illustrated in Fig. 11, the joint effects of NFETs leakage and IR drop undergo notable changes. NFETs leakage increases fourfold, concurrently with an increase in IR drop. IR drop can be disregarded at $r = 0.1 \Omega$, so the shift from $N_r = 256$ to 1024 primarily reflects the impact of the elevated overall NFETs leakage current, as depicted in Fig. 11 (a). It also shows that for $R_{off} > 1 M\Omega$, IR drop becomes negligible. Thus, within the range of $R_{off} > 1 M\Omega$, the changes in Fig. 11 (b) due to the scaling up of router size is solely attributable to the increase in overall NFETs leakage currents. Furthermore, $I_{cc,leak}/I_{off}$ is decreased by over 50% compared to the ideal case when $R_{off} > 10 M\Omega$ (e.g., $I_{cc,leak}/I_{off} < 5$ at $N_r = 1024$, $N_{SI} = 10$). Consequently, NFETs leakage becomes predominant when $R_{off} > 10 M\Omega$.

In addition, the leakage currents indicate a design trade-off for 1T1R arrays between area and leakage power consumption from transistors in 22 nm technology and beyond: if using high V_T FETs for lower leakage, bigger size is required to achieve higher driving ability for memristor programming.

CONCLUSIONS

We determined specifications for enabling the scaling of memristor crossbar routers with theoretical considerations and

simulation studies, and validated them with experimental measurements performed on a 4K-ReRAM chip. We configured the chip to implement a crossbar router and demonstrated experimentally its limits in transmitting spikes for SNN neuromorphic architectures. The routing error probability caused by current accumulation from “off” cells and the effect of the IR drop on metal lines is evaluated. We showed how the IR drop decreases the read margin (on/off ratio), and increases the error probability. We proposed an analytic model that can be used to guide future development of memristive devices for these use cases. We concluded that, for the examples at 22 nm technology node, a resistance range of LRS $> 50 k\Omega$ with on/off ratio > 20 is ideal. Our study also indicates a design trade-off between area and leakage power consumption.

REFERENCES

- [1] G. Indiveri, B. Linares-Barranco, R. Legenstein, G. Deligeorgis, and T. Prodromakis, “Integration of nanoscale memristor synapses in neuromorphic computing architectures,” *Nanotechnology*, vol. 24, no. 38, p. 384010, sep 2013. [Online]. Available: <https://dx.doi.org/10.1088/0957-4484/24/38/384010>
- [2] P. Yao, H. Wu, B. Gao, S. B. Eryilmaz, X. Huang, W. Zhang, Q. Zhang, N. Deng, L. Shi, H.-S. P. Wong *et al.*, “Face classification using electronic synapses,” *Nature communications*, vol. 8, no. 1, pp. 1–8, 2017.
- [3] Q. Xia, W. Robinett, M. W. Cumbie, N. Banerjee, T. J. Cardinali, J. J. Yang, W. Wu, X. Li, W. M. Tong, D. B. Strukov *et al.*, “Memristor-cmos hybrid integrated circuits for reconfigurable logic,” *Nano letters*, vol. 9, no. 10, pp. 3640–3645, 2009.
- [4] Y. Y. Liao, Z. Zhang, W. Kim, A. E. Gamal, and S. S. Wong, “Non-volatile 3d-fpga with monolithically stacked rram-based configuration memory,” in *2012 IEEE International Solid-State Circuits Conference*, 2012, pp. 406–408.
- [5] X. Tang, E. Giacomini, P. Cadareanu, G. Gore, and P.-E. Gaillardon, “A rram-based fpga for energy-efficient edge computing,” in *2020 Design, Automation & Test in Europe Conference & Exhibition (DATE)*, 2020, pp. 144–a–144–f.
- [6] T. Dalgaty, F. Moro, Y. Demirag, A. De Pra, G. Indiveri, E. Vianello, and M. Payvand, “The neuromorphic mosaic: re-configurable in-memory small-world graphs,” 2021.
- [7] K. Boahen, “Point-to-point connectivity between neuromorphic chips using address events,” *IEEE Transactions on Circuits and Systems II: Analog and Digital Signal Processing*, vol. 47, no. 5, pp. 416–434, 2000.
- [8] N. Kim, T. Austin, D. Baauw, T. Mudge, K. Flautner, J. Hu, M. Irwin, M. Kandemir, and V. Narayanan, “Leakage current: Moore’s law meets static power,” *Computer*, vol. 36, no. 12, pp. 68–75, 2003.
- [9] J. Chen, C. Wu, G. Indiveri, and M. Payvand, “Reliability analysis of memristor crossbar routers: Collisions and on/off ratio requirement,” in *2022 29th IEEE International Conference on Electronics, Circuits and Systems (ICECS)*, 2022, pp. 1–4.
- [10] Y. Liao, B. Gao, F. Xu, P. Yao, J. Chen, W. Zhang, J. Tang, H. Wu, and H. Qian, “A compact model of analog rram with device and array nonideal effects for neuromorphic systems,” *IEEE Transactions on Electron Devices*, vol. 67, no. 4, pp. 1593–1599, 2020.
- [11] Q. Qin, B. Gao, Q. Liu, Z. Liu, Y. Lin, P. Yao, Y. Zhou, R. Yu, Z. Hao, J. Tang, Q. Zhang, L. Dai, Z. Su, Q. Xu, S. You, H. Wu, and H. Qian, “Hybrid precoding with a fully-parallel large-scale analog rram array for 5g/6g mimo communication system,” in *2022 International Electron Devices Meeting (IEDM)*, 2022, pp. 33.2.1–33.2.4.
- [12] J. Liang, S. Yeh, S. S. Wong, and H.-S. P. Wong, “Effect of wordline/bitline scaling on the performance, energy consumption, and reliability of cross-point memory array,” *J. Emerg. Technol. Comput. Syst.*, vol. 9, no. 1, feb 2013. [Online]. Available: <https://doi.org/10.1145/2422094.2422103>
- [13] S. Moradi, N. Qiao, F. Stefanini, and G. Indiveri, “A scalable multicore architecture with heterogeneous memory structures for dynamic neuromorphic asynchronous processors (dynaps),” *IEEE Transactions on Biomedical Circuits and Systems*, vol. 12, no. 1, pp. 106–122, 2018.